Optics Letters

Graphene-based plasmonic modulator on a groove-structured metasurface

YULIN WANG, TAO LI,* AND SHINING ZHU

China National Laboratory of Solid State Microstructures, School of Physics, College of Engineering and Applied Sciences, Collaborative Innovation Center of Advanced Microstructures, Nanjing University, Nanjing 210093, China
**Corresponding author: taoli@nju.edu.cn*

Received 11 April 2017; revised 9 May 2017; accepted 9 May 2017; posted 11 May 2017 (Doc. ID 292704); published 6 June 2017

Graphene holds great potential to provide efficient modulation in optoelectronic integrated circuits due to its excellent tunability in conductivity, and several types of graphene-based photonic modulators have already been demonstrated. In this Letter, a plasmonic modulator was proposed based on a groove-structured metasurface covered by a single-layer graphene sheet, in which a transverse electrical-like mode is accommodated. Our design takes advantage of the field enhancement of the plasmonic mode and overcomes the orientation mismatch between the electrical field of the free surface plasmons and the graphene plane. Therefore, this graphene-based plasmonic modulator exhibits a greatly improved modulation depth, compared with the conventional plasmonic ones. Our theoretical results also show that this modulator can work in a broadband with acceptable insertion loss, indicating possible applications in nanophotonic integrations.

OCIS codes: (250.5403) Plasmonics; (160.3918) Metamaterials; (250.4110) Modulators.

https://doi.org/10.1364/OL.42.002247

An optical modulator is a key component in photonic integrations. Along with many progresses to the high efficient modulations, graphene has arrested many researchers attention due to its striking properties (e.g., high electron mobility and excellent electrical tunability), which have been used to achieve efficient optoelectronic devices (sensors, photodetectors, etc.) [1–4]. The conductivity of graphene can be modified by means of chemical doping, externally employed electric or magnetic fields, which benefit for realizing compact optical modulators [5–8]. A high-speed graphene-based optical modulator in silicon waveguide was successfully obtained [9]. In despite of further progress by adding more layers of graphene to enhance the modulation depth [10], the weak evanescent field outside the dielectric waveguides still limits its efficient interaction with graphene. Afterwards, there were some other designs proposed addressing this issue to improve the performance of an optical modulator, e.g., by placing graphene at the maximum of the electric field inside the waveguides [5,11], or employing a microcavity to enhance the light-graphene interactions [12,13]. Nevertheless, these designs still either remain challenges in experiments or have further upgrade possibilities.

A surface plasmonic polariton (SPP) is a confined optical field bounded on the metal surface with a compressed wavelength, which is regarded as a promising carrier to downsize the conventional optical components to the nanoscale [14–17]. Its highly confined electric field would be in favor of enhancing the interaction between the SPP field and graphene as is placed on the metal surface, since they are dimensionally matched to a 2D plane. Therefore, combining the graphene to an SPP device will possibly enhance the light-graphene interaction and would be a promising way to improve modulator efficiency. Unfortunately, a graphene-based SPP modulator has been experimentally demonstrated with a very low modulation depth of 1.4×10^{-4} dB/μm [18]. It is because the dominating field of SPP is out of plane that contributes little to the in-plane conductivity of graphene. Although the authors in [18] improved the modulation depth by introducing the corrugated SPPs and wedge SPPs, the performances are still worse than in a Si waveguide system and do not reach the expectation.

In principle, a basic method to enhance the interaction between a SPP and graphene is to convert the orientation of a major electric field from normal to parallel to the graphene plane [19]. Here, we proposed a design of plasmonic metasurface with a nano-groove array, on which a graphene sheet is covered with electrodes for externally gate voltage tuning, as schematically shown in Fig. 1. Through careful analysis, an appropriate plasmonic mode is found to be suitable for graphene modulation with transverse electric (TE)-polarized excitation, which shows greatly enhanced modulation depth, broadband property, and relatively acceptable insertion loss. Such a groove-structured metasurface would possibly provide people a good graphene-based platform for new explorations in developing optoelectronic functionalities and devices with enhanced light-matter interactions.

Figure 1 schematically shows the design of a plasmonic modulator based on a groove-structured metasurface with a single-layer graphene sheet. This metasurface is constructed by an array of periodic subwavelength grooves on a silver film in which the width of the grooves is defined as d, the depth is defined as h, and the period is defined as p (see the cross section

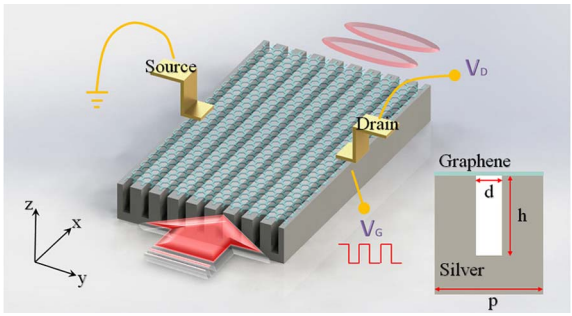

Fig. 1. Schematics of a groove-structured metasurface with graphene on it. The inset is the cross section of the unit cell with parameters marked out.

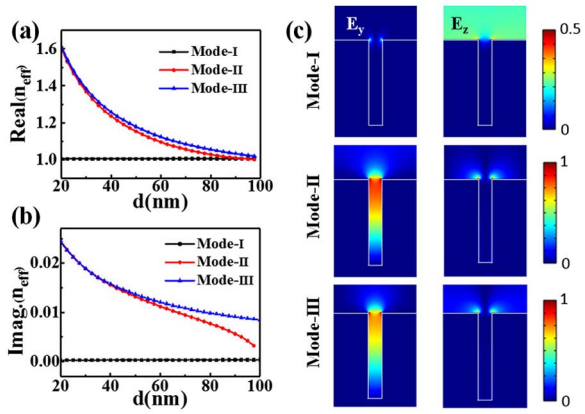

Fig. 2. (a), (b) Real and imaginary part of the effective mode index with respect to a different groove width (d). (c) Simulated field distributions (the parallel E_y and normal E_z components) in the cross section for the three modes with widths of 80 nm.

in the insert figure). Since such a groove-structured metasurface is actually a composition of well-arranged groove waveguides, the electromagnetic mode supported on this metasurface can be investigated with respect to the eigenmodes of the groove waveguide with a periodic boundary condition. Thanks to the coupling of the two sides of the silver grooves, the electrical field may be confined around the groove with a major component in the y direction. When a single sheet of graphene is placed on top of the silver grooves, there will be a dominant component electric field (E_y) parallel to the graphene sheet that matches the direction of the graphene plane. It should be additionally noted that in some literature the graphene was theoretically defined as an isotropic material, in which an epsilon-near-zero effect was observed that accounts for a very strong modulation capability [20–22]. However, further analyses [23] and experimental results [18] did not confirm this property, and an anisotropic graphene model with in-plane conductivity we used here should be the correct one.

In order to explore the optical property of this groove-structured metasurface, a commercial solution based on a finite element method (COMSOL 4.2a) was employed to study the eigenmodes of the grooved waveguides without graphene. At a working wavelength of $\lambda_0 = 1550$ nm, it is found of three eigenmodes. Here, we fixed the period ($p = 500$ nm) and depth ($h = 500$ nm), and studied the influence of the groove width (d) on the mode properties. Figures 2(a) and 2(b), respectively, depict the real and imaginary parts of the effective mode indices (n_{eff}) as functions of the groove width. It is apparently observed that Mode-II and Mode-III strongly depend on the groove width, while Mode-I is almost unchanged, which possibly indicates that Mode-II and Mode-III are groove SPP modes, and Mode-I is not. By checking the mode distributions for the case of $d = 80$ nm [see Fig. 2(c)], we will find that Mode-I exhibits a very weak electric field (both E_y and E_z) inside the groove, and has a predominant normal field (E_z) on top of the metal layer, which actually implies that this mode is a conventional SPP mode on top of a flat silver surface. The simulated mode effective index (n_{eff}) is $1.0047 + 0.0034i$ in coincidence with the theoretical data ($1.0040 + 0.0028i$) of a free SPP on a flat metal surface calculated by $n_{\text{eff}} = k_{\text{spp}}/k_0 = [(\epsilon_m\epsilon_d)/(\epsilon_m + \epsilon_d)]^{1/2}$ with ϵ_m defined by a Drude model of silver [24].

Mode-II and Mode-III show a strongly enhanced parallel electric field (E_y) inside the groove that confirms both groove SPP modes and guarantees the strong interaction of these E_y fields with the graphene sheet at top of the groove. Though the E_y field does not spread over the entire silver surface, the greatly enhanced field in the y direction matching the planar conductivity of graphene would possibly improve the modulation performance. By carefully comparing Mode-II and Mode-III, we will find that Mode-II has two nodes of the E_z field at the boundaries of the unit cell, indicating a same phased E_z field in the neighboring unit. However, Mode-III has a non-zero E_z extending to the boundaries that implies an anti-phased E_z distribution in neighbor. Correspondingly, the E_y field inside the grooves of two neighboring units should be in-phase for Mode-II and anti-phase for Mode-III. In fact, Mode-II and Mode-III can be regarded as the symmetric (even) and anti-symmetric (odd) groove modes in this metasurface. Considering a possible experimental excitation, the in-phase Mode-II is more accessible by introducing a TE polarization to this metasurface, and the anti-phased Mode-III is hard to obtain. Therefore, we will mainly investigate Mode-II for the function of a plasmonic modulator. According to Figs. 2(a) and 2(b), the mode indices of both Mode-II and III increase with reducing the groove width and tend to degenerate, which can be explained that more confinement of an electric field inside the narrow groove will reduce the coupling of two neighboring grooves and leads to identical symmetric and anti-symmetric modes. On the other hand, when we enlarge the groove width d, the mode indices decrease and even become the same as the free SPP (Mode-I). In consideration of a proper propagating loss and experimental feasibility, a suitable groove width was finally chosen to be 80 nm in the following investigations.

Based on such a groove-structured metasurface as a substrate, a single-layer graphene sheet, which is treated as a conductivity surface in the COMSOL modeling, was then placed on top of the metasurface with a thin dielectric spacer. In this design, the silver metasurface can act as another role of electrode as a bottom gate. Here, we performed simulations on such a graphene-covered metasurface with a 7 nm thick Al_2O_3 spacer and found that the mode properties change little, compared with the bare metasurface analyzed above. It is ready to accept that influence from the ultrathin dielectric spacer and the graphene sheet is very weak. Nevertheless, the propagating loss arising from the in-plane conductivity of graphene would change with the chemical potential (i.e., Fermi energy E_f)

tuned by applied gate voltage. It is rightly the function of the modulator that we expected.

The dynamic in-plane conductivity $\sigma(\omega)$ of graphene is derived from the Kubo formula with both intraband and interband contributions [25,26]. Assuming $k_B T \ll |E_f|$ and $\hbar\omega$, the intraband contribution can be simplified into the Drude-like form [27,28]:

$$\sigma_{\text{intra}}(\omega) = \frac{je^2 E_f}{\pi\hbar^2(\omega + j\tau^{-1})}, \tag{1}$$

and the interband conductivity can be approximated as [25,26]

$$\sigma_{\text{inter}}(\omega) = \frac{je^2}{4\pi\hbar} \ln\left(\frac{2|E_f| - (\omega + j\tau^{-1})\hbar}{2|E_f| + (\omega + j\tau^{-1})\hbar}\right), \tag{2}$$

where e is the charge of an electron, $\hbar = h/2\pi$ is the reduced Planck constant, ω is the radian frequency, k_B is Boltzmann's constant, T is the temperature, $E_f = \hbar V_f(\pi n)^{1/2}$ is Fermi energy (i.e., chemical potential), n is the carrier density, and $V_f \approx 1 \times 10^6$ m/s is the Fermi velocity in graphene. The carrier density can be changed by gating $n = \epsilon_0\epsilon_d V_g/(ed)$; d is the thickness of the spacer layer ($d = 7$ nm); and $\epsilon_d = 9$ for Al_2O_3. The carrier relaxation time τ is determined by the carrier mobility μ in graphene as $\tau = \mu E_f/eV_f^2$, where μ of graphene ranges from ~1000 $cm^2/(V \cdot s)$ in chemical vapor deposition grown graphene [29] to 23,000 $cm^2/(V \cdot s)$ in suspended exfoliated graphene [30]. The gate-dependent complex permittivity of graphene $\epsilon(\omega)$ was obtained from the complex conductivity $\sigma(\omega) = \sigma_{\text{intra}}(\omega) + \sigma_{\text{inter}}(\omega)$ according to the intraband and interband contributions. Using a moderate mobility of 3000 $cm^2/(V \cdot s)$ and a changing E_f, the gate-dependent complex dielectric function of graphene was calculated as the real and imaginary parts shown in Figs. 3(a) and 3(b), respectively.

At a low doping concentration, by applying a low driving voltage ($V_g < 1.7$ V), the Fermi energy of graphene locates at a proper level within the threshold ($E_f < \hbar\omega/2 = 0.4$ eV), and the electron interband transition occurs as pumped by the external photon, including a surface plasmon; thus, the optical mode should exhibit a relatively large loss with a large imaginary mode index. Here, the excitation of the groove SPP with primary E_y leads to a much stronger interaction with graphene than that of the free SPP on the flat metal, so that the mode loss corresponding to the imaginary part of n_{eff} is much larger than Mode-I at low drive voltage [see Fig. 3(d)]. As for heavy doping cases, the Fermi energy will exceed the transition threshold ($E_f > \hbar\omega/2$) owing to the positive charge accumulation, which leads to an abrupt decrease in the imaginary part of graphene permittivity. As a result, there is no electron available for interband transition, and the graphene appears to be nearly transparent with a greatly reduced propagation loss. After tuning the Fermi energy, the real part [Fig. 3(c)] and imaginary part [Fig. 3(d)] of the effective mode indices change. The change of Imag. (n_{eff}) provides a change of propagation loss, from which the modulation depth (M_d) can be calculated according to $M_d = [10 \lg(I_{\text{OFF}}/I_{\text{ON}})]/L$. Here, the modulation depth of Mode-II is calculated showing a value of about **0.40 dB/μm**, which is in the same order as that of Mode-III and three orders higher than Mode-I (as well as the free SPP reported in [18]).

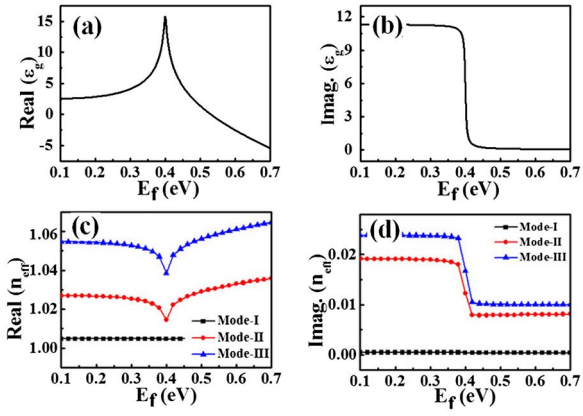

Fig. 3. (a), (b) Real and imaginary parts of in-plane permittivity of graphene. (c), (d) Real and imaginary parts of the effective mode index with respect to the Fermi energy.

In order to confirm the mode analyses results, a 3D propagation simulation for Mode-II was further carried out, by which the modulation depth can be directly calculated according to the change of field intensities after a certain propagating distance. The calculated transmission data (after a propagating distance of 8 μm) of the groove SPP (Mode-II) are plotted in Fig. 4(a) with respect to different Fermi energy, which shows a similar curve as the imaginary mode index [see Fig. 3(d)]. From the data, a preferable modulation depth of **0.38 dB/μm** is obtained that agrees well with the mode analyses result. The simulated field propagations with states of "OFF" ($E_f = 0.3$ eV) and "ON" ($E_f = 0.5$ eV) shown in the insert figures in Fig. 4(a), from which a distinct intensity contrast can be observed at the end of the propagations. According to the transmission of the ON state, the mode loss can be obtained with an acceptable low value as 0.43 dB/μm.

By further comparative calculations on the metasurface with graphene involved or not, we obtained a considerably low insertion loss of 5.6×10^{-3} dB/μm in this system, which is quite acceptable with respect to its modulation depth. Moreover, this modulator demonstrates a broadband property after more detailed investigations, as the results shown in Fig. 4(b). The black line represents the transmission coefficient of the "OFF" state ($E_f = 0.3$ eV), and the red one shows the "ON" state ($E_f = 0.5$ eV) with the incident wavelength changing from 1200 to 1700 nm. The refractive index of silver is calculated according to the Drude model with $\omega_p = 1.37 \times 10^{16}$ rad/s and $\gamma = 8.5 \times 10^{13}$ rad/s [31]. The blue line

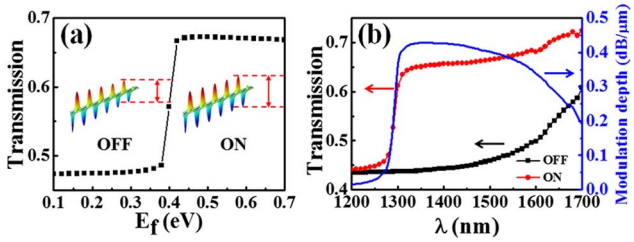

Fig. 4. (a) Transmission curve with respect to different E_f calculated by 3D propagation simulations, in which the "OFF" ($E_f = 0.3$ eV) and "ON" ($E_f = 0.5$ eV) states are depicted. (b) Transmission spectra of "OFF" (black square) and "ON" (red circle) states from $\lambda = 1200$–1700 nm, where the modulation depth is also displayed (blue curve).

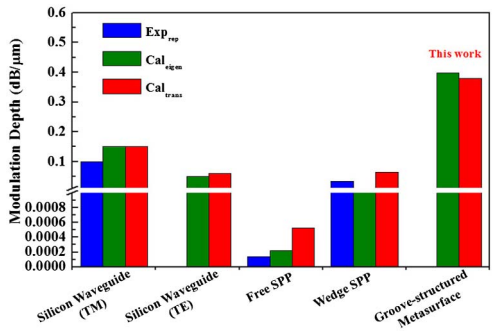

Fig. 5. Bar graph for comparison of the data of optical modulation depth. Here, the blue bars are from the experimental data reported for the silicon waveguide (TM mode) [9], free SPP and wedge SPP [18]; the green and red bars are our calculation results by eigenmode analyses and propagation simulations, respectively.

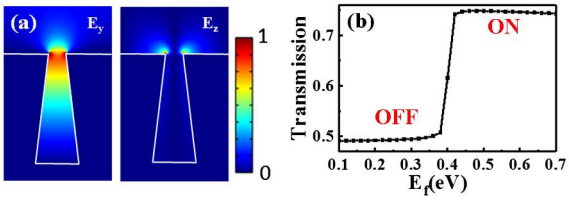

Fig. 6. Results of a tapered groove structure with bottom size of groove of 200 nm. The groove SPP mode will have an enhanced electric field E_y at the upper entrance due to a coupling effect, which gives rise to an improved modulation depth of 0.47 dB/μm and a lower mode loss of 0.31 dB/μm.

depicts the modulation depth within this wavelength range, which indicates that this plasmonic modulator has a preferable performance between 1300 and 1600 nm.

Additionally, we further studied the modulation performance by mode analyses and transmission calculation on the graphene-loaded silicon waveguide [9] and plasmonic system [18] for comparison with our results, among which our design shows an obvious advantage in modulation depth (see Fig. 5). It should be noted that the proposed groove-structured metasurface provides a more electrically matched platform for graphene modulation with TE-polarized excitation, which can be further optimized in the groove geometry (see Fig. 6).

In conclusion, we proposed a graphene-based plasmonic modulator on a groove-structured metasurface, exhibiting 10 × higher modulation depth compared to plasmonic modulators reported recently. By comparison with other graphene-based modulators, our design demonstrated obviously improved performance. Moreover, its broadband property, acceptable structural parameters, and insertion loss promise the realization in experiments. Our design makes good use of plasmonic field enhancement and field orientation conversion, and would possibly inspire new fruitful possibilities in developing nanophotonic devices as new 2D materials are involved.

Funding. National Program on Key Basic Research Project of China (2016YFA0202103); National Natural Science Foundation of China (NSFC) (11322439, 11621091, 11674167).

Acknowledgment. Y. L. Wang is grateful for the support from the Scientific Research Foundation of the Graduate School of Nanjing University. T. Li is grateful for the support from Dengfeng Project B of Nanjing University.

REFERENCES

1. G. T. Reed, G. Mashanovich, F. Y. Gardes, and D. J. Thomson, Nat. Photonics **4**, 518 (2010).
2. A. Liu, R. Jones, L. Liao, D. Samara-Rubio, D. Rubin, O. Cohen, R. Nicolaescu, and M. Paniccia, Nature **427**, 615 (2004).
3. R. Jacobsen, K. Andersen, P. Borel, J. Fage-Pedersen, L. Frandsen, O. Hansen, M. Kristensen, A. Lavrinenko, G. Moulin, H. Ou, C. Peucheret, B. Zsigri, and A. Bjarklev, Nature **441**, 199 (2006).
4. F. Bonaccorso, Z. Sun, T. Hasan, and A. C. Ferrari, Nat. Photonics **4**, 611 (2010).
5. K. Kim, J. Y. Choi, T. Kim, S. H. Cho, and H. J. Chung, Nature **479**, 338 (2011).
6. Q. Bao and K. P. Loh, ACS Nano **6**, 3677 (2012).
7. A. Vakil and E. Nader, Science **332**, 1291 (2011).
8. R. Li, M. Imran, X. Lin, H. Wang, Z. Xu, and H. Chen, Nanoscale **9**, 1449 (2017).
9. M. Liu, X. Yin, E. Ulin-Avila, B. Geng, T. Zentgraf, L. Ju, F. Wang, and X. Zhang, Nature **474**, 64 (2011).
10. M. Liu, X. Yin, and X. Zhang, Nano Lett. **12**, 1482 (2012).
11. X. Yin, T. Zhang, L. Chen, and X. Li, Opt. Lett. **40**, 1733 (2015).
12. X. Gan, K. F. Mak, Y. Gao, Y. You, F. Hatami, J. Hone, T. F. Heinz, and D. Englund, Nano Lett. **12**, 5626 (2012).
13. X. T. Gan, R. J. Shiue, Y. D. Gao, K. F. Mak, X. W. Yao, L. Z. Li, A. Szep, D. Walker, J. Hone, T. F. Heinz, and D. Englund, Nano Lett. **13**, 691 (2013).
14. N. Yu and F. Capasso, Nat. Mater. **13**, 139 (2014).
15. A. V. Kildishev, A. Boltasseva, and V. M. Shalaev, Science **339**, 1232009 (2013).
16. Y. Fu, X. Hu, C. Lu, S. Yue, H. Yang, and Q. Gong, Nano Lett. **12**, 5784 (2012).
17. Y. L. Wang, T. Li, L. Wang, H. He, L. Li, Q. J. Wang, and S. N. Zhu, Laser Photon. Rev. **8**, L47 (2014).
18. D. Ansell, I. Radko, Z. Han, F. Rodriguez, S. Bozhevolnyi, and A. Grigorenko, Nat. Commun. **6**, 8846 (2015).
19. I. Radko, S. Bozhevolnyi, and A. Grigorenko, Opt. Express **24**, 8266 (2016).
20. Z. Lu and W. Zhao, J. Opt. Soc. Am. B **29**, 1490 (2012).
21. J. Gosciniak and D. T. Tan, Sci. Rep. **3**, 1897 (2013).
22. S. Lee, T. Q. Tran, M. Kim, H. Heo, J. Heo, and S. Kim, Opt. Express **23**, 33350 (2015).
23. M. S. Kwon, IEEE Photon. J. **6**, 1 (2014).
24. S. A. Maier, *Plasmonics: Fundamentals and Applications* (Springer, 2007).
25. N. M. R. Peres, F. Guinea, and A. H. Castro Neto, Phys. Rev. B **73**, 125411 (2006).
26. V. P. Gusynin, S. G. Sharapov, and J. P. Carbotte, Phys. Rev. Lett. **96**, 256802 (2006).
27. M. Jablan, H. Buljan, and M. Soljacic, Phys. Rev. B **80**, 245435 (2009).
28. G. W. Hanson, J. Appl. Phys. **104**, 084314 (2008).
29. L. Ju, B. S. Geng, J. Horng, C. Girit, M. Martin, Z. Hao, H. A. Bechtel, X. G. Liang, A. Zettl, Y. R. Shen, and F. Wang, Nat. Nanotechnol. **6**, 630 (2011).
30. K. I. Bolotin, K. J. Sikes, Z. Jiang, M. Klima, G. Fudenberg, J. Hone, P. Kim, and H. L. Stormer, Solid State Commun. **146**, 351 (2008).
31. T. Li, H. Liu, S. M. Wang, X. G. Yin, F. M. Wang, S. N. Zhu, and X. Zhang, Appl. Phys. Lett. **93**, 021110 (2008).